Monthly Notices
of the
ROYAL ASTRONOMICAL SOCIETY

Mon. Not. R. Astron. Soc. **416,** 3057–3066 (2011) doi:10.1111/j.1365-2966.2011.19252.x

A study of relative velocity statistics in Lagrangian perturbation theory with PINOCCHIO

Lavinia Heisenberg,[1,2]★ Björn Malte Schäfer[3] and Matthias Bartelmann[2]

[1]*Département de Physique Théorique, Université de Genève, 24, quai E. Ansermet, 1211 Genève, Switzerland*
[2]*Institut für theoretische Astrophysik, Zentrum für Astronomie, Universität Heidelberg, Albert-Ueberle-Straße 2, 69120 Heidelberg, Germany*
[3]*Astronomisches Recheninstitut, Zentrum für Astronomie, Universität Heidelberg, Mönchhofstraße 12, 69120 Heidelberg, Germany*

Accepted 2011 June 14. Received 2011 June 3; in original form 2010 November 6

ABSTRACT

Subject of this paper is a detailed analysis of the PINpointing Orbit-Crossing Collapsed HIerarchical Object (PINOCCHIO) algorithm for studying the relative velocity statistics of merging haloes in Lagrangian perturbation theory. Given a cosmological background model, a power spectrum of fluctuations as well as a Gaussian linear density contrast field δ_1 is generated on a cubic grid, which is then smoothed repeatedly with Gaussian filters. For each Lagrangian particle at position $\boldsymbol{q}$ and each smoothing radius R, the collapse time, the velocities and ellipsoidal truncation are computed using Lagrangian perturbation theory. The collapsed medium is then fragmented into isolated objects by an algorithm designed to mimic the accretion and merger events of hierarchical collapse. Directly after the fragmentation process the mass function, merger histories of haloes and the statistics of the relative velocities at merging are evaluated. We reimplemented the algorithm in C++, recovered the mass function and optimized the construction of halo merging histories. When compared with the output of the Millennium Simulation our results suggest that the PINOCCHIO is well suited for studying relative velocities of merging haloes and is able to reproduce the pairwise velocity distribution.

Key words: methods: analytical – methods: numerical – large-scale structure of Universe.

1 INTRODUCTION

To account for structure formation, one needs to develop techniques for studying the non-linear evolution of perturbations. In the strongly non-linear regime, where the perturbation amplitudes exceed unity ($|\delta| \gg 1$), the linear approximation breaks down and has to be replaced by other approaches. To accentuate the need for this, one has to look at the interesting structures in the Universe, like galaxies or clusters of galaxies because they are highly non-linear. Since every theory of structure formation must be capable of describing the formation and evolution of non-linear objects, the major developments occurred in perturbation theory and numerical simulations. It has been understood that this aim simplifies when formulated in terms of Lagrangian coordinates rather than the standard Eulerian ones, since the latter one relies on physical densities being small (Bouchet et al. 1992; Buchert 1992). So one assumes that the dynamics of gravitational clustering is described more suitably in terms of the displacement field $\boldsymbol{D}$, which is the only underlying fundamental field in the Lagrangian approach. The decisive difference to the Eulerian approach is that it is not based on the smallness of the density of the inhomogeneities and that one searches for solutions of perturbed trajectories about the linear initial displacement $\boldsymbol{D}^{(1)}$ (Sahni & Coles 1995; Ehlers & Buchert 1997; Bernardeau et al. 2002). The fundamental point is that a small perturbation of the Lagrangian particle paths carries a large amount of non-linear information about the corresponding Eulerian-evolved observables, since the Lagrangian picture is intrinsically non-linear in the density field. Lagrangian perturbation theory reaches its limit of applicability when trajectories of particles cross and the mapping from the initial conditions to the evolved density field cease to be unique. This defines the so-called orbit crossing which is numerically achieved by means of the ellipsoidal collapse approximation to the full Lagrangian perturbative expansion. These collapsed objects can then be grouped into disjoint haloes and their relative velocities can be measured.

There are a number of applications of large simulated volumes with velocity information: for instance, simulations of redshift–space distortions in the galaxy correlation function, investigations of large-scale bulk flows (Zaroubi et al. 2002), which offer a possibility of testing modified gravity models (Ayaita, Weber & Wetterich 2009), and testing the occurrence of high-velocity merging events, such as the bullet cluster, which is the topic of recent controversies (Hayashi & White 2006). Many cluster observables such as the strong-lensing cross-section (Torri et al. 2004; Fedeli et al. 2006) and the radio and X-ray luminosity (Randall, Sarazin & Ricker

★E-mail: lavinia.heisenberg@unige.ch

2002) are boosted during the merging process, and for treating these systems, statistical information about the merging configuration is needed.

The cosmological model used is a spatially flat Λ cold dark mater (ΛCDM) cosmology with Gaussian adiabatic initial perturbations in the CDM density field with the following cosmological parameter set $(\Omega_{m0}, \Omega_\Lambda, h, \sigma_8) = (0.25, 0.75, 0.73, 0.9)$, identical to that used in the Millennium Simulation, with which we will compare our results. Our computational domain is a cubic box of size 256 Mpc h^{-1} with periodic boundary conditions filled with $N^3 = 128^3$ particles.

2 COSMOLOGY

In this first introductory section, we summarize all the known formulae we use to compute the power spectrum and the Gaussian linear density contrast field. The linear CDM power spectrum $P(k)$ describes the fluctuation amplitude of the Gaussian initial density field δ, $\langle\delta(\boldsymbol{k})\delta(\boldsymbol{k}')\rangle = (2\pi)^3\delta_D(\boldsymbol{k}+\boldsymbol{k}')P(k)$, and is given by the ansatz

$$P(k) \propto k^{n_s} T^2(k), \tag{1}$$

with the transfer function $T(k)$ which is approximated by (Bardeen et al. 1986),

$$T(q) = \frac{\ln(1+aq)}{aq}(1 + bq + (cq)^2 + (dq)^3 + (eq)^4)^{-\frac{1}{4}}. \tag{2}$$

In the transfer function, the wavenumber $k = q\Gamma$ is rescaled by the shape parameter Γ (Sugiyama 1995),

$$\Gamma = \Omega_\mathrm{m} h \exp\left(-\Omega_\mathrm{b}\left(1 + \frac{\sqrt{2h}}{\Omega_\mathrm{m}}\right)\right). \tag{3}$$

For further treatment, one introduces the smoothed density field δ_R, which is averaged on the scale R,

$$\tilde{\delta}_R(\boldsymbol{k}) = \tilde{\delta}(\boldsymbol{k})\tilde{W}_R(\boldsymbol{k}), \tag{4}$$

and for the smoothed power spectrum

$$P_R(k) = |\tilde{W}_R(k)|^2 P(k), \tag{5}$$

with the window function, $W_R(r)$, satisfying $\int \mathrm{d}^3x\, W_R(|\boldsymbol{x}|) = 1$. There exist several choices for the window function W_R, a very common one is the top-hat filter, which is given by

$$\tilde{W}_R(k) = 3\frac{\sin(kR) - kR\cos(kR)}{(kR^3)}. \tag{6}$$

Using the definitions introduced so far, it is now straightforward to calculate the variance $\sigma^2(R) = \langle\delta_r^2(\boldsymbol{x})\rangle$ of the smoothed density field as

$$\sigma^2(R) = \int \frac{\mathrm{d}^3k}{(2\pi)^3} P_R(k) = \int \frac{\mathrm{d}^3k}{(2\pi)^3} |\tilde{W}_R(k)|^2 P(k), \tag{7}$$

which we use to fix the normalization to $\sigma^2(R = 8\ \mathrm{Mpc}\, h^{-1}) \equiv \sigma_8^2$.

3 LAGRANGIAN PERTURBATION THEORY

In this section, we summarize the idea and results of the Lagrangian perturbation theory, which we use to study the dynamical equations of the considered non-linear system. The formation of CDM haloes involves highly non-linear dynamical processes, which can only be followed in numerical simulations or by applying perturbative methods. As mentioned in the introduction, one important approach is Lagrangian perturbation theory. In order to describe the non-linear dynamical evolution of the particle trajectories up to third order of Lagrangian coordinates, the following three steps have to be followed.

(i) Description of the mapping from the Eulerian to the Lagrangian coordinates.

(ii) Transformation of the Eulerian fields to Lagrangian coordinates.

(iii) Application of perturbation theory to the Lagrangian equations expressed by the displacement up to the desired order.

The starting point is a pressureless, non-vertical, self-gravitating fluid with Newtonian gravity embedded in an expanding Friedmann–Lemaître–Robertson–Walker universe (Bouchet et al. 1992). In the Lagrangian framework of fluid dynamics, the relation between the Eulerian position $\boldsymbol{x}$ of a mass particle and the initial Lagrangian position $\boldsymbol{q}$ is given by the displacement field (Zel'dovich 1970):

$$\boldsymbol{x}(\boldsymbol{q}, t) = \boldsymbol{q} + \boldsymbol{D}(\boldsymbol{q}, t). \tag{8}$$

In the Lagrangian space, the trajectories of the mass elements are fully described by the dynamical mappings $\boldsymbol{x}(\boldsymbol{q}, t)$, starting from the initial positions $\boldsymbol{q}$.

There is a one-to-one correspondence between the Langrangian coordinate $\boldsymbol{q}$ and the Eulerian coordinate $\boldsymbol{x}$ for a cold non-collisional fluid, at least until the stage of caustic formation. Expressed mathematically, this corresponds to the statement that the functional determinant J of the Jacobian of the mapping relation $\boldsymbol{q} \to \boldsymbol{x}(\boldsymbol{q}, t)$ is non-singular,

$$J(\boldsymbol{q}, t) \equiv \det\left(\frac{\partial \boldsymbol{x}}{\partial \boldsymbol{q}}\right) \neq 0, \tag{9}$$

which means that the mapping $\boldsymbol{x}(\boldsymbol{q}, t)$ is invertible to $\boldsymbol{q}(\boldsymbol{x}, t)$. It is evident that many particles coming from very different original positions will tend to arrive at the same Eulerian position during the highly non-linear evolution. As a consequence of that infinite-density regions (caustics) will be formed in Eulerian space. Hence the mapping from Lagrangian to Eulerian space becomes singular and the density becomes infinite due to the proportionality $\rho \propto J^{-1}$. Since the displacement $\boldsymbol{D}$ fully characterizes the mapping between the Eulerian and the Lagrangian coordinates, the motion of the fluid elements is completely described in terms of it. One can now express the peculiar velocity, acceleration and density contrast by inserting the displacement field $\boldsymbol{D}$ into the Euler and the continuity equations. Similarly, the Eulerian irrotationality condition and the Poisson equation can be written in terms of the displacement (Catelan 1995) resulting in the dynamical equations for the displacements $\boldsymbol{D}$. The fundamental question now is how to solve the dynamical equations for the displacements $\boldsymbol{D}$. The irrotationality condition and the Lagrangian Poisson equation are exact equations in the Lagrangian description. It is undoubtedly very difficult to solve them in a rigorous way. A possible alternative is to seek for approximate solutions. The standard technique is to expand the trajectory $\boldsymbol{D}$ in a perturbative series, with the leading term being the linear displacement which corresponds to the Zel'dovich approximation (Zel'dovich 1970; Bouchet et al. 1992). Approximating the Lagrangian Poisson equation implies that the gravitational interaction among the particles of the fluid is described by the first few terms of a Taylor expansion:

$$\boldsymbol{D}(\boldsymbol{q}, \tau) = g_1(\tau)\boldsymbol{D}^{(1)}(\boldsymbol{q}) + g_2(\tau)\boldsymbol{D}^{(2)}(\boldsymbol{q}) + \cdots, \tag{10}$$

with $\boldsymbol{D}^{(n)}(\boldsymbol{q})$ being the nth-order approximation. The dynamics of the evolution constrains in general both the temporal dependence as described by the functions, g_n, and the spatial displacements $\boldsymbol{D}^{(n)}(\boldsymbol{q})$. The displacement fields are computed considering the potential of a homogeneous ellipsoid in its principal axis frame

$\psi(\boldsymbol{q}) = \frac{1}{2}(\lambda_1 q_1^2 + \lambda_2 q_2^2 + \lambda_3 q_3^2)$, solving the Poisson and irrotationality condition equations in Lagrangian space, where the λ_i are the eigenvalues of the first-order deformation tensor $\psi_{,ab}(\boldsymbol{q})$. The solutions can be found in Catelan (1995) and Monaco (1997a,b) to which we refer for all details. We use the results from Monaco (1997a) for the calculation of collapse times $J(\boldsymbol{q}, g_c) = 0$:

$$1 + \lambda_i g_c - \frac{3}{14}\lambda_i(\delta_l - \lambda_i) g_c^2 + \left(\frac{I_3}{126} + \frac{5}{84}\lambda_i \delta_l(\delta_l - \lambda_i)\right) g_c^3 = 0. \quad (11)$$

Just in order to give some examples, the first-order collapse time is given by $g_c^{(1)} = -\frac{1}{\lambda_3}$, whereas the second-order solution results to be $g_c^{(2)} = \frac{7\lambda_3 + \sqrt{7\lambda_3(\lambda_3 + 6\delta_l)}}{3\lambda_3(-\lambda_3 + \delta_l)}$ (and analogously for the third order, see Monaco 1997a).

3.1 PINOCCHIO

A compromise between simulations and analytical techniques is a perturbative approach describing the growth of haloes in a given numerical realization of a linear density field such as the truncated Zel'dovich approximation and the PINpointing Orbit-Crossing Collapsed HIerarchical Objects (PINOCCHIO) algorithm (Taffoni, Monaco & Theuns 2002). PINOCCHIO is an algorithm for studying the formation and evolution of dark matter haloes in a given initial linear density field, which we outline briefly in this section. It was first developed by Monaco, Theuns & Taffoni (2002). Local parametrizations to the dynamics are used to give precise predictions of the hierarchical formation of dark matter haloes when the correlations in the initial density field are properly taken into account Fig. 1 summarizes the function of PINOCCHIO and shows how the formation of haloes is modelled on the formation of the large-scale structure, which is computed by Lagrangian perturbation theory.

This modus operandi enables the automatic generation of a large ensemble of accurate halo merging histories and additionally delivers their spatial distribution. Likewise, the approach can be efficiently applied for generating the input for galaxy formation models, since the properties of the halo population are of fundamental importance for understanding galaxy formation and evolution.

PINOCCHIO consists of two steps which determine the hierarchical formation of haloes through accretion and merging.

(i) The first step handles the definition of the collapse time. Hereby, orbit crossing will be identified as the instant when a mass element undergoes collapse, without the need to introduce a free parameter. Orbit crossing is numerically calculated by means of the ellipsoidal collapse approximation to the full Lagrangian perturbative expansion, as discussed in the previous section (Monaco 1995).

(ii) The second step groups the collapsed particles into disjoint haloes, applying an algorithm similar to that used to identify haloes in n-body simulations.

As explained in the previous subsection, the density diverges as the Jacobian determinant vanishes, corresponding to the formation of a caustic, which means that particle trajectories cross and the transformation $\boldsymbol{x} \rightarrow \boldsymbol{q}$ becomes multivalued. Since the density

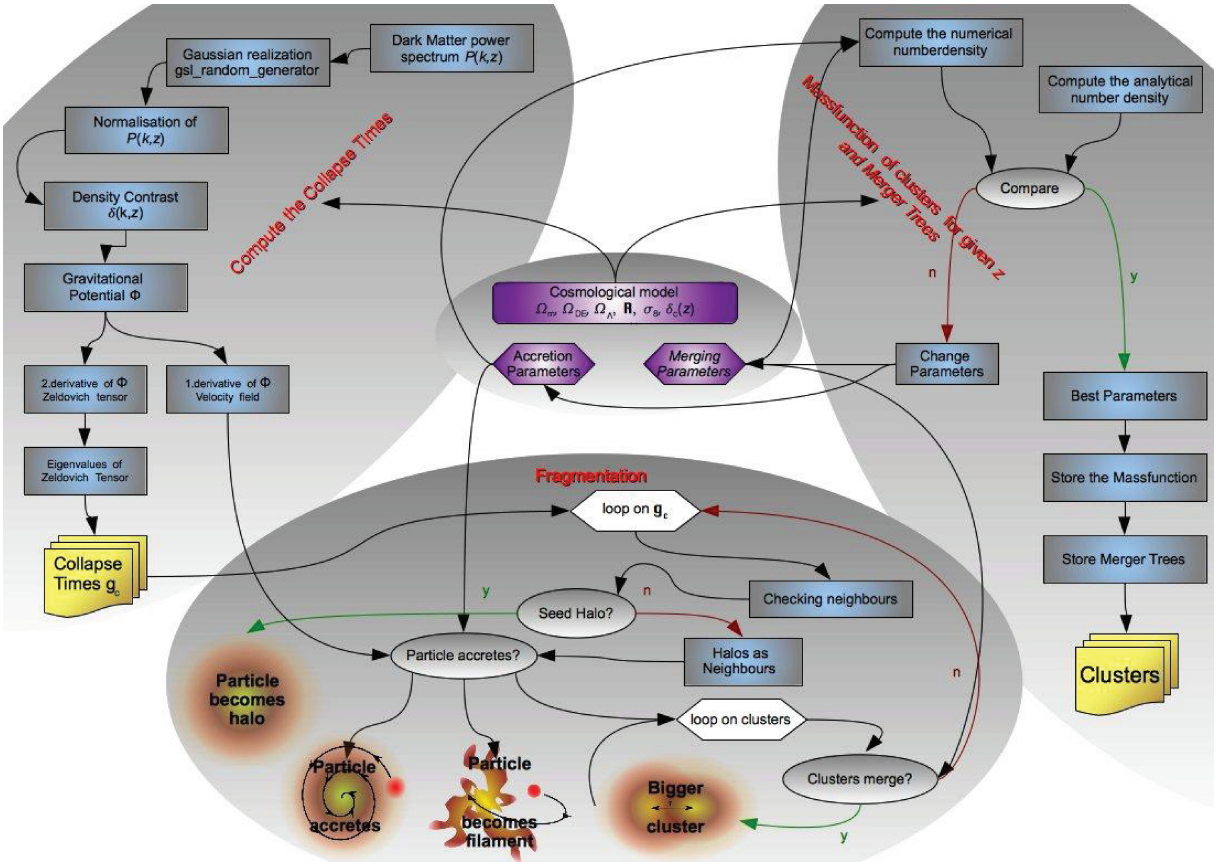

Figure 1. Flow chart of the code: the main three blocks of the code are shown. For a given set of parameters (centre), we compute the collapse times (top-left) and for each collapsing particle we apply the fragmentation procedure (bottom). Finally, we analyse the statistical properties of the fragmented objects (top-right).

becomes very high at orbit crossing, this event will be identified as the collapse time. In this manner, it is very easy to compute collapse using Lagrangian perturbation theory which remains valid up to that particular instant but breaks down afterwards.

The hierarchical formation of objects is done due to the grouping of orbit-crossing particles into haloes by tracing the merging processes for each particle individually. Briefly, two main processes contribute to the hierarchical clustering: the first one is the accretion of particles on to haloes and the second one is the merging of haloes. For this purpose, the particles of the realization are sorted in chronological order of collapse. Starting with the earliest collapse time, the particles are assigned either to a halo or to filaments at the corresponding collapse times. In order for a collapsing particle to be accreted by a halo, it must fulfil a number of conditions. One of them is that the candidate halo must already contain one of its six nearest neighbours in the Lagrangian space of initial conditions. The fragmentation process contains four different cases, which are sufficient for performing the identification and merging history of haloes (Fig. 2).

If none of the six Lagrangian neighbours has collapsed, then the particle is a local maximum of the inverse collapse time. This particle is a seed for a new halo having the unit mass of the particle and is created at the particle's position. Obviously, the earliest particle to collapse is the first halo.

In the case that the collapsing particle touches only one halo, then the accretion condition, if the halo is close enough, is checked. When the accretion condition is satisfied, then the particle is added to the halo; otherwise, it is marked as belonging to a filament. Thus, not every collapsed particle becomes a relaxed halo, but can be tagged as a filament. The particles that only touch filaments are marked as filaments as well. If the collapsing particle has more than one touching halo as Lagrangian neighbour, then the merging condition is checked for all halo pairs. Pairs that satisfy the conditions are merged. The accretion condition for the particle is checked for all touching haloes both before and after merging. In the case that the particle can accrete to both haloes, without the haloes merging, it accretes on to that halo for which the distance d in units of halo size R_N is smaller. It may happen that particles fail to accrete even though the haloes merge.

If the collapsing particle does not accrete on to the candidate haloes in the case they are too far, it becomes a filament. But later for this filament particle there is still the possibility to accrete when its neighbouring particle accretes on to a halo. This is done in order to mimic the accretion of filaments on to the haloes. Note that up to five filament particles can flow into a halo at each accretion event.

3.2 Velocity statistics

In the Eulerian specification of the flow field, the flow quantities are depicted as functions of fixed position $\boldsymbol{q}$ and time t. The peculiar velocity expressed in terms of the displacement field $\boldsymbol{D}$ in the Lagrangian specification of the flow field would then be

$$\boldsymbol{v}(t) = \dot{\boldsymbol{x}}(t) = \dot{g}(t)\boldsymbol{D}(\boldsymbol{q}). \tag{12}$$

Now let us study the time evolution of two elements positioned at the Lagrangian coordinates $\boldsymbol{q}_a$ and $\boldsymbol{q}_b$. The Eulerian positions and peculiar velocities at these two points are then given as

$$\boldsymbol{x}_a \equiv \boldsymbol{x}_a(\boldsymbol{q}_a, t) = \boldsymbol{q}_a + g(t)\boldsymbol{D}(\boldsymbol{q}_a) \equiv \boldsymbol{q}_a + g(t)\boldsymbol{D}_a, \tag{13}$$

$$\boldsymbol{x}_b \equiv \boldsymbol{x}_b(\boldsymbol{q}_b, t) = \boldsymbol{q}_b + g(t)\boldsymbol{D}(\boldsymbol{q}_b) \equiv \boldsymbol{q}_b + g(t)\boldsymbol{D}_b, \tag{14}$$

$$\boldsymbol{v}_a(t) \equiv \boldsymbol{v}_a(\boldsymbol{q}_a, t) = \dot{g}(t)\boldsymbol{D}_a, \tag{15}$$

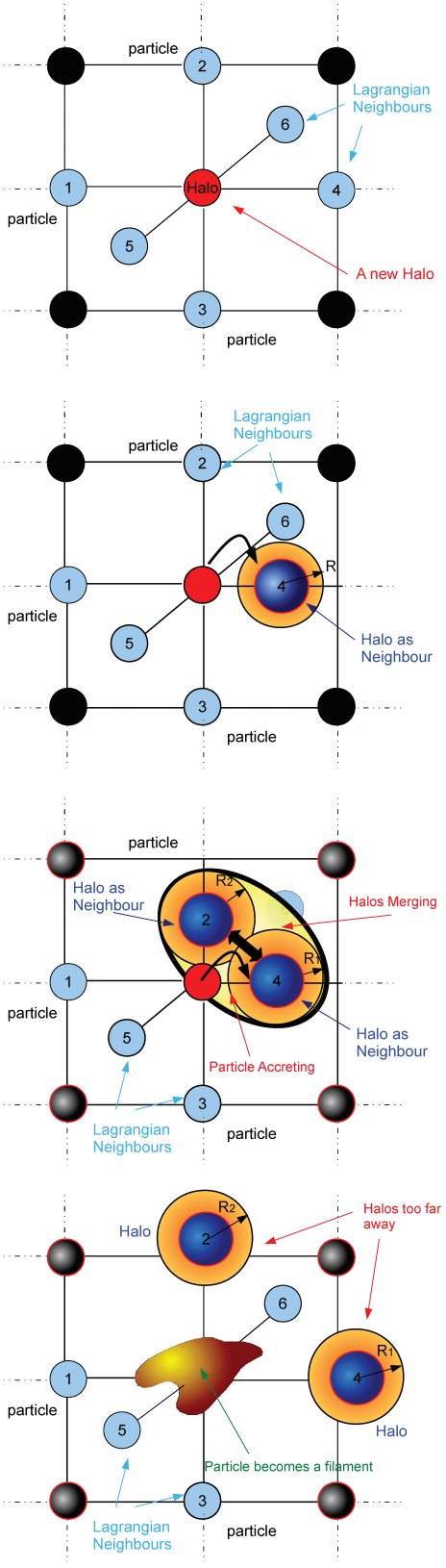

Figure 2. Cases of the fragmentation process: the top panel shows the six Lagrangian neighbours of a given particle, the second panel illustrates how this particle accretes on to a neighbouring halo, the third panel depicts the merging of two haloes and successive accretion and, if there is no accretion, the particle is marked as belonging to a filament in the bottom panel.

$$\boldsymbol{v}_b(t) \equiv \boldsymbol{v}_b(\boldsymbol{q}_b, t) = \dot{g}(t)\boldsymbol{D}_b. \tag{16}$$

The relative velocity of the two particles is given by

$$\boldsymbol{v}_{ab} = \boldsymbol{v}_b(t) - \boldsymbol{v}_a(t) = \dot{g}(t)(\boldsymbol{D}_b - \boldsymbol{D}_a) \equiv \boldsymbol{v}_\parallel(t) + \boldsymbol{v}_\perp(t), \tag{17}$$

where $\boldsymbol{v}_\parallel(t)$ and $\boldsymbol{v}_\perp(t)$ stand for the components parallel and perpendicular to $\boldsymbol{r}_{ab}(t) \equiv \boldsymbol{x}_b(t) - \boldsymbol{x}_a(t)$. We can now compute the probability distribution function (PDF) of the pairwise peculiar velocity $\boldsymbol{v}$ with separation $\boldsymbol{s}$ from the initial PDF as (Seto & Yokoyama 1998)

$$P(\boldsymbol{v}, \boldsymbol{s}, t) = \frac{1}{4\pi s^2} \int 4\pi r^2 \mathrm{d}r\, \mathrm{d}v_{\parallel i} \mathrm{d}v_{\perp xi} \mathrm{d}v_{\perp yi}\, p(v_{\parallel i}, v_{\perp xi}, v_{\perp yi}; r) \times \delta(s - r_{ab}(t))\delta(v - v_{\parallel i}(t)), \tag{18}$$

where $p(v_{\parallel i}, v_{\perp xi}, v_{\perp yi}; r)$ is the initial PDF which depends only on $\boldsymbol{v}_{\parallel i}$ and $\boldsymbol{v}_{\perp i} \equiv \sqrt{v_{\perp xi}^2 + v_{\perp yi}^2}$, where $v_{\perp xi}$ and $v_{\perp yi}$ are the two components of $\boldsymbol{v}_{\perp i}$ perpendicular to each other. The subscript i denotes quantities at some initial time. Fig. 3 shows the geometrical configuration with a definition of all necessary quantities.

Putting the Eulerian positions and peculiar velocities into the above PDF gives

$$P(\boldsymbol{v}, \boldsymbol{s}, t) \propto \int_{r^\star}^{\infty} r\mathrm{d}r p\left(v_{\parallel i}^\star, v_{\perp i}^\star; r\right), \tag{19}$$

where $v_{\parallel i}^\star$ and $v_{\perp i}^\star$ stand for

$$v_{\parallel i}^\star \equiv \frac{\dot{g}_i}{g}\left(\frac{s^2}{r} - \frac{sg}{r\dot{g}}v - r\right), \tag{20}$$

$$v_{\perp i}^\star \equiv \frac{\dot{g}_i}{g} s\left(1 - \frac{s^2}{r^2} - \frac{g^2}{r^2\dot{g}^2}v^2 + \frac{sg}{r^2\dot{g}}v\right), \tag{21}$$

$$r^\star \equiv \left|s - \frac{g}{\dot{g}}v\right|. \tag{22}$$

We have to specify the initial PDF $p(v_{\parallel i}^\star, v^\star{}_{\perp i}; r)$ in order to be able to compute the desired PDF $P(\boldsymbol{v}, \boldsymbol{s}, t)$. As we were dealing with the longitudinal mode, the peculiar velocity in the linear regime is related to the $\delta(\boldsymbol{x}, t)$ and accordingly to its Fourier transform $\delta_{\boldsymbol{k}}(t)$:

$$\boldsymbol{v}(\boldsymbol{x}, t) = \mathrm{i}\frac{\dot{g}_i}{g_i} \int \frac{\boldsymbol{k}}{k^2} \delta_{\boldsymbol{k}}(t_i) \mathrm{e}^{\mathrm{i}\boldsymbol{k}\boldsymbol{x}} \frac{\mathrm{d}^3k}{(2\pi)^3}. \tag{23}$$

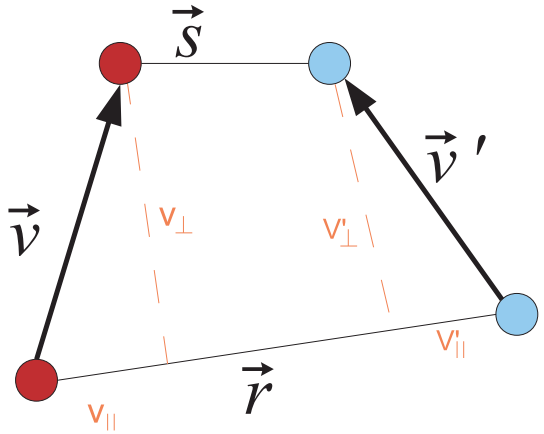

Figure 3. The visualisation of the configuration.

It is important to emphasize that the initial pairwise peculiar velocities are Gaussian distributed like the initial density fluctuations. From the velocity correlation tensor $\langle v_a v_b \rangle$ one obtains the projections

$$\langle v_\parallel v_\parallel \rangle = \sum_{a,b} \left(r_a^\parallel r_b^\parallel - \frac{1}{3}\delta_{ab}\right) \langle v_a v_b \rangle, \tag{24}$$

$$\langle v_\perp v_\perp \rangle = \sum_{a,b} \left(r_a^\perp r_b^\perp - \frac{1}{3}\delta_{ab}\right) \langle v_a v_b \rangle. \tag{25}$$

Thus, the two-point correlation functions are given by (Gorski 1988)

$$\langle v_{\parallel i} v_{\parallel i} \rangle = \frac{1}{6\pi^2}\left(\frac{\dot{g}_i}{g_i}\right)^2 \int \mathrm{d}k P_i(k) \left(1 - 3j_0(kr) + 6\frac{j_1(kr)}{kr}\right) \tag{26}$$

$$\langle v_{\perp i} v_{\perp i} \rangle = \frac{1}{6\pi^2}\left(\frac{\dot{g}_i}{g_i}\right)^2 \int \mathrm{d}k P_i(k) \left(1 - 3\frac{j_1(kr)}{kr}\right). \tag{27}$$

Finally, the initial PDF is given by

$$p(v_{\parallel i}^\star, v_{\perp i}^\star; r) = \frac{\mathrm{e}^{-T}}{\sqrt{(2\pi)^3 Y_\parallel(r) Y_\perp^2(r)}}, \qquad T \equiv \frac{\left(v_{\parallel i}^\star\right)^2}{2Y_\parallel(r)} + \frac{\left(v_{\perp i}^\star\right)^2}{2Y_\perp(r)}, \tag{28}$$

where $\langle v_{\parallel i} v_{\parallel i} \rangle \equiv Y_\parallel(r)$ and $\langle v_{\perp i} v_{\perp i} \rangle \equiv Y_\perp(r)$. Therefore, we can now obtain the desired PDF $P(\boldsymbol{v}, \boldsymbol{s}, t)$ through the integration $P(\boldsymbol{v}, \boldsymbol{s}, t) \propto \int_{r^\star}^{\infty} r\ \mathrm{d}r p(v_{\parallel i}^\star, v_{\perp i}^\star; r)$. We relate the distance $\boldsymbol{r}$ in the analytical model to the distance of two haloes at the time of merging. Furthermore, we substitute for the power spectrum a filtered spectrum smoothed at a wavelength which corresponds to the halo mass. Computing the velocity distribution at a distance $\boldsymbol{s}$ corresponding to the merging condition yields distributions very similar to those obtained by PINOCCHIO. In particular, we confirm the trend of steeper distributions at a lower mass ratio.

In particular, we confirm the trend of steeper distributions at a lower mass ratio, as can be seen in Fig. 4. This reflects the fact that merging processes in PINOCCHIO conserve momentum but not energy since merging is an inelastic collision. At each merging, the velocity of the final halo is given by $v_f = (v_1 m_1 + v_2 m_2)/(m_1 + m_2)$

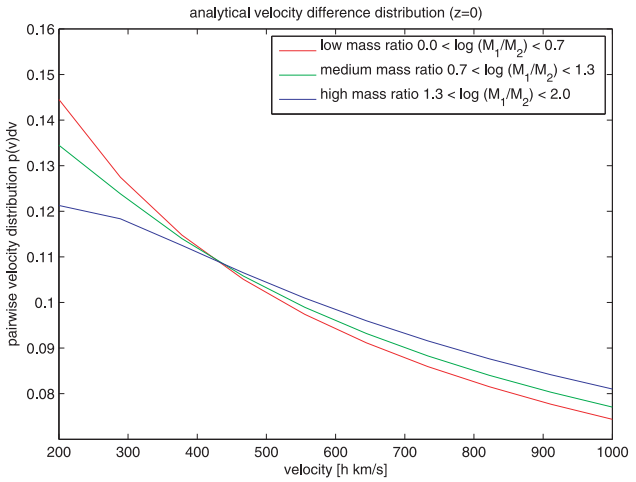

Figure 4. The analytical pair velocity probability density for three intervals in the mass ratio: the low-mass ratio $0.0 < \log(M_1/M_2) < 0.7$ (red line), the intermediate-mass ratio $0.7 < \log(M_1/M_2) < 1.3$ (green line) and the high-mass ratio $1.3 < \log(M_1/M_2) < 2.0$ (blue line).

since the momentum is conserved. Because of the energy loss high velocities do not appear in the PINOCCHIO velocity distribution and therefore the curve decreases faster. But the loss of energy does not occur in the analytical configuration and therefore the curve is shallower.

4 RESULTS

In the following, we present the results from a simulation for 128^3 particles in a box of side length $256\,\mathrm{Mpc}\,h^{-1}$, carried out in the framework of Lagrangian perturbation theory with our C++ reimplementation of the PINOCCHIO code for following the merging activity of the large-scale structure. There is always the problem of the coherence of the velocity field on large scales. For that reason, large simulation boxes are always preferred for the investigation of velocity statistics. Due to non-linear mode coupling even large modes influence the dynamics on small scales (Cole 1997), although this coupling decreases proportional to the inverse wavenumber or faster in classical perturbation theory. This difficulty can in principle be treated with PINOCCHIO using the method described by Monaco et al. (2005), which consists in adding large-scale modes to the Gaussian initial conditions; furthermore, a volume of size $256\,\mathrm{Mpc}\,h^{-1}$ has been demonstrated to sample the velocity field sufficiently well, as velocity differences are much less dependent on large-scale modes than velocities. Heuristically, the velocity difference statistic is closely related to that of the velocity field divergence, and has therefore the same properties as the density field itself, which is well sampled by our volume.

The first step was to create a realization of a Gaussian density field for a specified ΛCDM spectrum. From the density contrast, the gravitational potential and Zel'dovich tensor were derived. Differentiations were performed again in Fourier space allowing us to recover the quantities with the minimum noise. For each point $\boldsymbol{q}$ of the Lagrangian initial coordinates and each smoothing radius R, the collapse time, determined by the time at which the particle is predicted to enter a high-density multistream region, and ellipsoidal truncation were then computed using Lagrangian perturbation theory. Determining the eigenvalues of the Zel'dovich tensor, it is straightforward to calculate the collapse times evaluating the expressions of the individual orders (11). For each particle, only the earliest collapse time is recorded with the corresponding smoothing radius and velocity. The third-order Lagrangian prescription improves the collapse times. The first axis to collapse is the one corresponding to the smallest λ_3 eigenvalue, indicating the convergence and the fact that the Zel'dovich approximation makes the largest contribution to collapse dynamics. The collapsed medium is then fragmented into isolated objects using the algorithm which we described above to mimic the accretion and merger events of hierarchical collapse. We distinguish between collapsed particles belonging to relaxed haloes or to lower density filaments using the accretion and merging conditions. Once the fragmentation process is completed, we studied the relative velocities of the haloes at merging.

Figs 5 and 6 illustrate structure formation dynamics in the Lagrangian picture: matter is transported out of initially underdense regions and is accumulated in superstructures, where merging is prominent due to the high particle density. In fact, the most massive objects are found in regions of converging velocities, a nice example of which can be found in the upper right front corner of the simulation cube. One sees coherent flow patterns on the scale of the correlation length of the density field. In the vicinity of massive

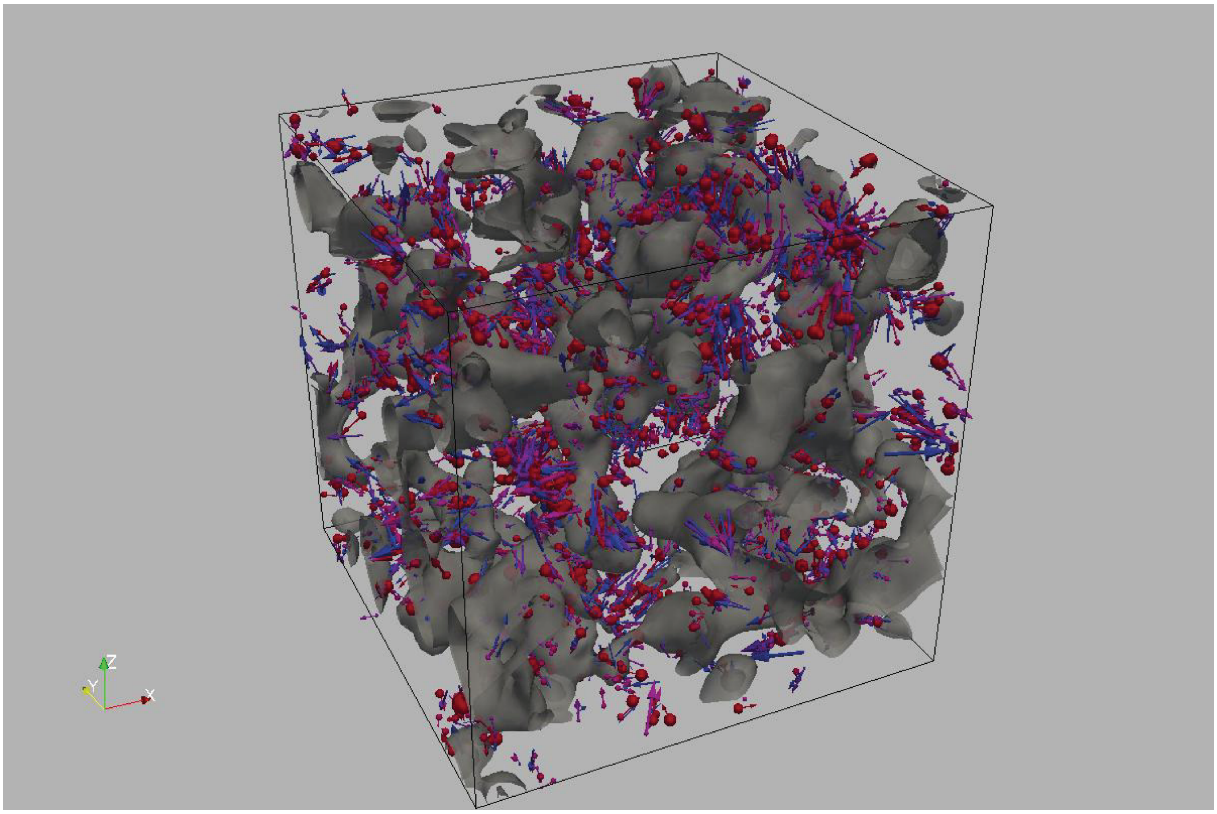

Figure 5. Density field, smoothed with a Gaussian kernel of $8\,\mathrm{Mpc}\,h^{-1}$, with contours at -2σ and -3σ, superimposed on the velocity field visualized by arrows and the halo distribution, where the size of the spheres is indicative of the logarithmic halo mass.

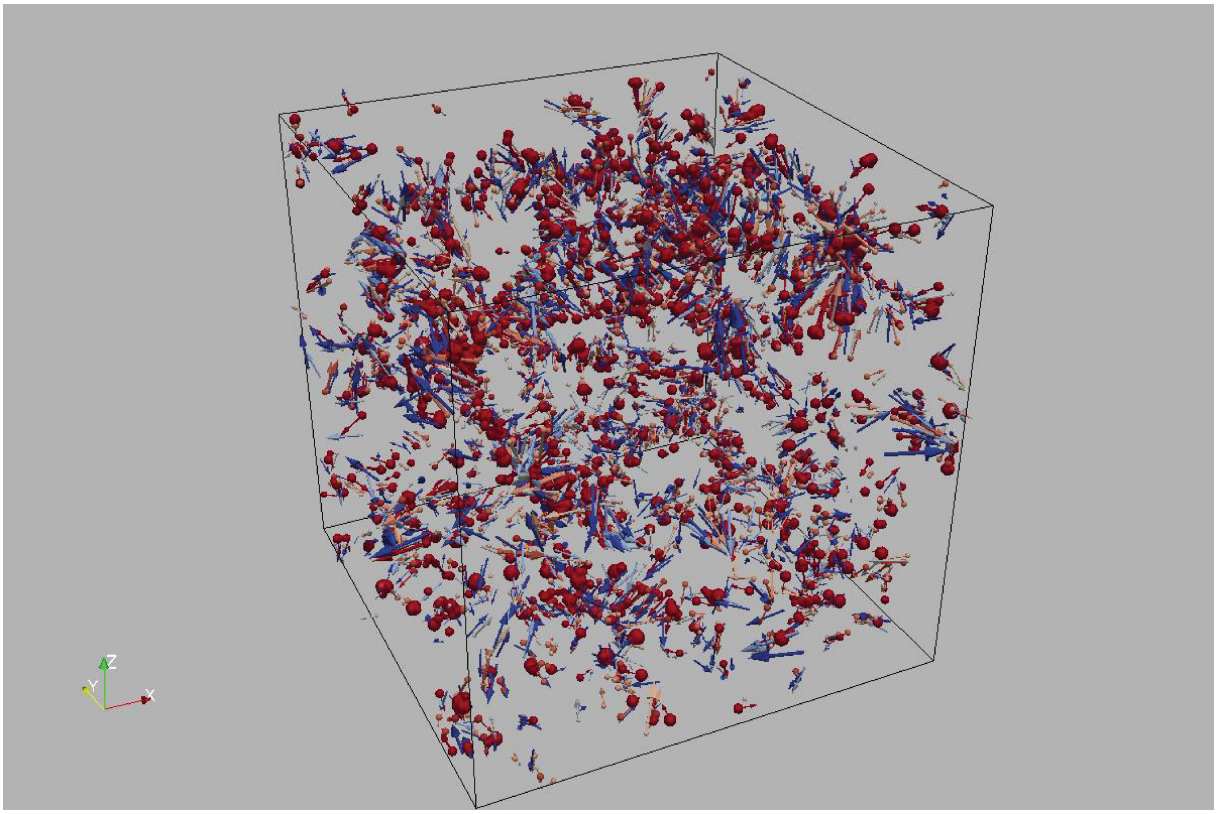

Figure 6. Similar to Fig. 5 only without isodensity contours for making the velocity field more visible. Logarithmic halo mass is indicated by size, and the arrow length is proportional to the halo velocity.

structures, one can observe larger relative velocities compared to underdense regions. This can be traced back to the fact that the velocity field of an overdense region has a larger variance compared to the cosmological average. The statistics of the velocity field is translated into that of the haloes by imposing momentum conservation in the merging process. Therefore, the figure confirms the expectation of high pairwise velocities in overdense regions.

In order to compare our results with the Millennium Simulation (Springel et al. 2005), we have applied the same merging conditions to the Millennium data. In Fig. 7, we compare the probability distribution of the relative velocity at the time of merging, for three different mass ratio intervals: approximately equal masses $\log(M_1/M_2) < 0.7$, intermediate values for the mass ratio $0.7 < \log(M_1/M_2) < 1.3$ and high-mass ratios $\log(M_1/M_2) > 1.3$. The data are further split into three redshifts: $z = 0$, 1, 2, while at higher redshifts the numbers of massive haloes are not sufficient for deriving the probability density as statistical error bars are too large to draw conclusions. The subdivision of the velocity range between 0 and 1000 km s^{-1} h^{-1} allows us to investigate the features of the velocity distribution while obtaining reasonable statistical error bars, and we normalize all histograms to unity. The error bars of the PINOCCHIO runs [$V = (256\,\mathrm{Mpc}\,h^{-1})^3$] are small enough to allow quantitative conclusions and are comparable to those from the Millennium data ($V = (256\,\mathrm{Mpc}\,h^{-1})^3$). For drawing velocity distributions, we selected haloes from mass intervals of identical width ranging from 4×10^{12} to $1 \times 10^{14}\,\mathrm{M}_\odot\,h^{-1}$.

For controlling the time-stepping, GADGET (which was used to carry out the Millennium Simulations) has a feature which synchronizes the individual time-steps for each particle prior to writing a simulation output at a pre-specified redshift. The PINOCCHIO simulation was stopped at the identical redshift, and given this approach, we do not expect difficulties to arise due to the time-discreteness of the Millennium output. Furthermore, as long as the structures are in the limit, where perturbation theory is applicable, which means that the trajectories of the particles can be extrapolated from the initial conditions, the choice of the time-stepping should not matter much, in contrast to non-linear structures with large gradients perpendicular to the particle trajectory.

A Metropolis–Hastings algorithm was used for checking the dependence of the mass function on the PINOCCHIO parameters, and we were able to reproduce mass functions in agreement with analytical functions for the proposed set of parameters. The influence of the parameter choice on the shape of the mass function was verified in our implementation, and the total number of haloes formed corresponds well to analytical expectations and the Millennium Simulation. For most of the tests presented in this paper, we used a Opteron 285 2.4 GHz 64-bit computer with a total memory of 8 GB. For example, resampling the initial conditions on to a 256^3 grid, the first step of initializing the Gaussian random field and computing the orbit crossing requires about 30 min of CPU time and the second part of identifying the haloes takes only a few additional minutes. Fig. 8 illustrates the agreement of the PINOCCHIO mass function with the analytical expectation.

Quite generally, the figures reproduce the basic behaviour expected from analytical arguments as outlined in Section 3.2. The distributions are steeper at a lower mass ratio in both the Millennium data set and in PINOCCHIO. The shape of the distributions between PINOCCHIO and the Millennium Simulation is very similar, particularly well at low redshifts, with the curves for the intermediate- and the high-mass ratio peaking at almost identical values for the

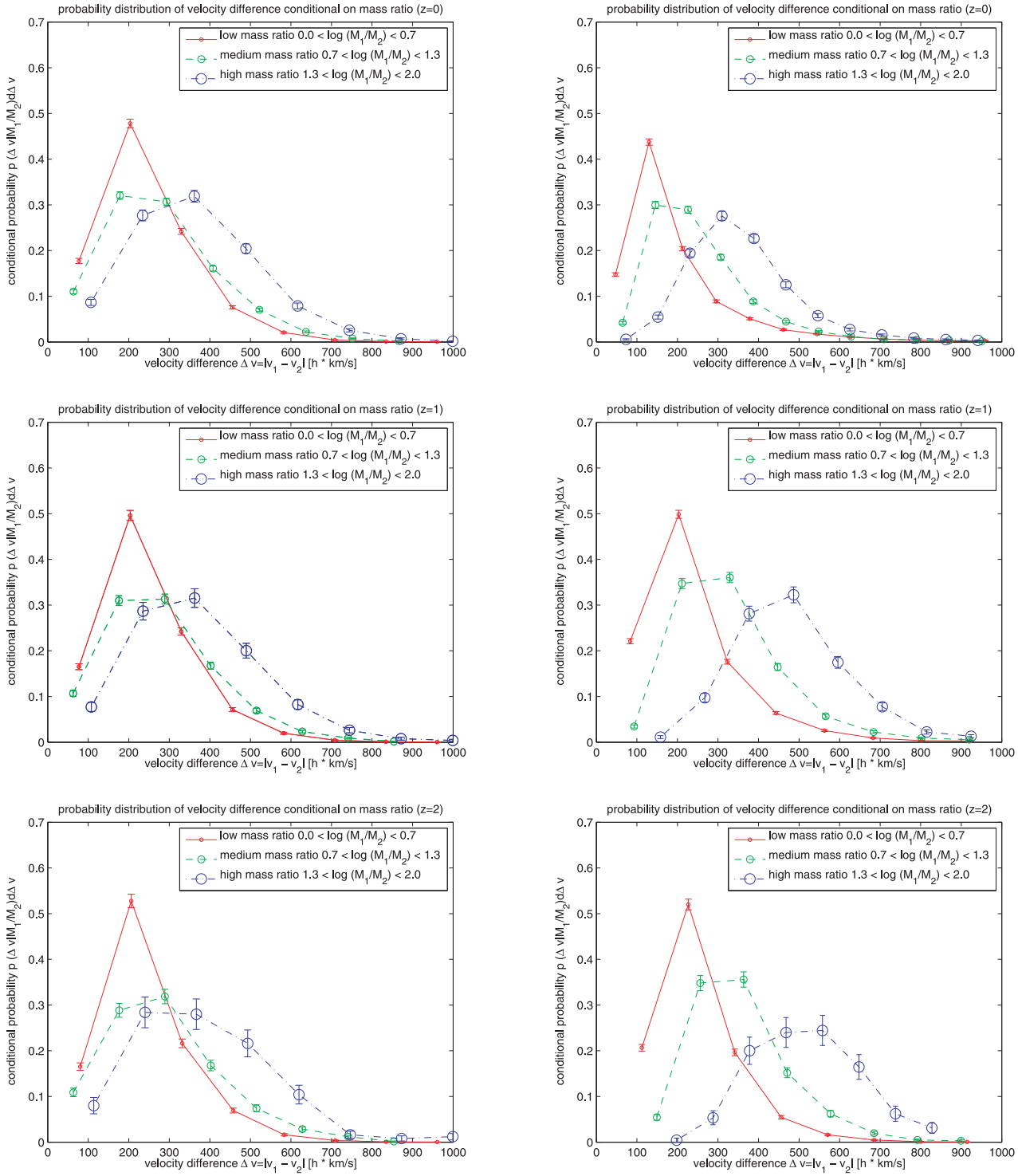

Figure 7. Probability distributions of velocities conditional on a halo mass ratio for redshift $z = 0$ (first row), $z = 1$ (second row) and $z = 2$ (third row), comparing PINOCCHIO (left-hand panel) with the Millennium Simulation (right-hand panel).

relative velocity. At high redshifts, PINOCCHIO underestimates the velocities in medium- and high-mass ratio mergers by a small amount. This underestimate is a known feature of Lagrangian codes and is discussed in the appendix of Monaco et al. (2005). All curves terminate at velocities of $\simeq$1000 km s^{-1} underlining the sparsity of high-velocity mergers (Hayashi & White 2006). Naturally, we expect the distributions of the Millennium Simulation to drop faster than corresponding distributions from PINOCCHIO because the latter treats merging processes as an inelastic collision and does not follow the dissipative dynamics inside haloes. Given the good agreement, we believe that halo velocity catalogues for a number of applications such as redshift space distortions, large-scale

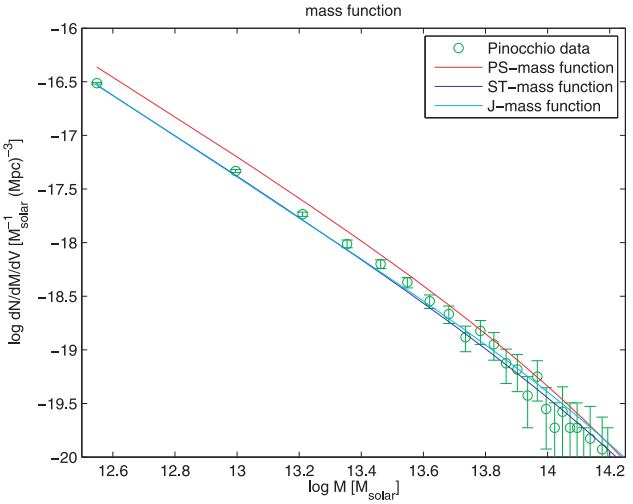

Figure 8. Comparison of the PINOCCHIO mass function with the analytical Press–Schechter, Sheth–Tormen and Jenkins mass functions.

bulk flows and merging processes, can be reliably derived from Lagrangian codes.

5 SUMMARY

The aim of this paper is to investigate merging processes in the cosmic large-scale structure in the framework of Lagrangian perturbation theory and to compare the results for the pairwise velocity distribution obtained with an adaptation of the PINOCCHIO algorithm to n-body data.

(i) It is comparatively simple in PINOCCHIO to construct merger trees as it is not necessary to identify haloes in the particle distribution and as one can directly follow the merging processes between haloes, such that the haloes in PINOCCHIO correspond to friends-of-friends particle groups in n-body simulations.

(ii) The halo's properties, such as the distribution of masses, spins and now also merger trees and pairwise velocities, can be reliably derived from a Lagrangian code, with the differences in the distribution being smaller than the statistical error bars. Hereby, we have investigated the derivation of the mass function from PINOCCHIO and used similar parameters as quoted by Monaco et al. (2002) for our studies of the velocity distributions. We have also investigated that the velocities show the correct scaling with cosmological parameters and the correct scaling with the halo mass ratio in comparison to an analytical calculation.

(iii) In comparison to an analytical pairwise velocity distribution, PINOCCHIO is able to reproduce the trend of shallower distributions with increasing halo mass ratio. At high velocities, however, PINOCCHIO exhibits a steeper behaviour compared to that predicted by the analytical calculation at a fixed mass ratio, which is explained by the fact that merging processes in PINOCCHIO are treated as inelastic collisions with conserved momentum but not conserved energy. Because of this energy loss, high velocities are not present in PINOCCHIO data and the distribution is steeper.

(iv) We find a general agreement between the velocity distributions of PINOCCHIO and the Millennium Simulation, both in terms of relative numbers and values for the absolute velocity. Additionally, the scaling with redshift and mass ratio between merging haloes behaves very similarly. The peaks of the distributions at low redshifts coincide with each other, and although distributions from the Millennium Simulation terminate earlier, this feature is not unexpected as PINOCCHIO does not treat the dissipative dynamics of merging haloes. Again, the correct dependence of pairwise velocity with halo mass ratio is recovered.

(v) PINOCCHIO, relying on a phenomenological description of the merging process of two haloes and combining the individual momenta in an inelastic collision is very fast compared to n-body codes, which allows sweeps in the parameter space relevant to peculiar velocities, i.e. Ω_m, σ_8 and the dark energy parameters, for which we have verified the basic relations expected by linear structure formation.

Further questions include the environment dependence of velocity statistics, which is comparatively easy to do in Lagrangian perturbation theory. A very useful discriminant for this purpose is the number of positive eigenvalues of the shear tensor. One would expect smaller velocities inside voids and larger velocities in supercluster regions. In fact, this dependence can already be seen in Fig. 5. Other extensions include the investigation of two-point statistics of the velocity field and to answer questions related to velocity statistics (Regos & Szalay 1995). In a future paper, we will investigate the dependence of the strong-lensing cross-section of merging systems with velocities drawn from PINOCCHIO-simulated volumes and its dependence on the choice of cosmological parameters.

Anaglyphic versions of Figs 5 and 6 are available on request from the authors.

ACKNOWLEDGMENTS

We thank Volker Springel for his suggestions and access to the Millennium data base. LH's work is partially funded by the SNF. BMS's work is supported by the Graduate School of Fundamental Physics in the framework of the DFG's Excellence Initiative. MB received funding from DFG's Transregio TR33. We appreciate the comments from our reviewer, Pierluigi Monaco. We would like to thank Francesco Pace for answering questions on the original FORTRAN code and Jean-Claude Waizmann for his suggestions to improve the figures.

REFERENCES

Ayaita Y., Weber M., Wetterich C., 2009, preprint (arXiv:0908.2903)
Bardeen J. M., Bond J. R., Kaiser N., Szalay A. S., 1986, ApJ, 304, 15
Bernardeau F., Colombi S., Gaztañaga E., Scoccimarro R., 2002, Phys. Rep., 367, 1
Bouchet F. R., Juszkiewicz R., Colombi S., Pellat R., 1992, ApJ, 394, L5
Buchert T., 1992, MNRAS, 254, 729
Catelan P., 1995, MNRAS, 276, 115
Cole S., 1997, MNRAS, 286, 38
Ehlers J., Buchert T., 1997, Gen. Relativ. Gravitation, 29, 733
Fedeli C., Meneghetti M., Bartelmann M., Dolag K., Moscardini L., 2006, A&A, 447, 419
Gorski K., 1988, ApJ, 332, L7
Hayashi E., White S. D. M., 2006, MNRAS, 370, L38
Monaco P., 1995, ApJ, 447, 23
Monaco P., 1997a, MNRAS, 287, 753
Monaco P., 1997b, MNRAS, 290, 439
Monaco P., Theuns T., Taffoni G., 2002, MNRAS, 331, 587
Monaco P., Møller P., Fynbo J. P. U., Weidinger M., Ledoux C., Theuns T., 2005, A&A, 440, 799
Randall S. W., Sarazin C. L., Ricker P. M., 2002, ApJ, 577, 579
Regos E., Szalay A. S., 1995, MNRAS, 272, 447
Sahni V., Coles P., 1995, Phys. Rep., 262, 1
Seto N., Yokoyama J., 1998, ApJ, 492, 421

Springel V. et al., 2005, Nat, 435, 629
Sugiyama N., 1995, ApJS, 100, 281
Taffoni G., Monaco P., Theuns T., 2002, MNRAS, 333, 623
Torri E., Meneghetti M., Bartelmann M., Moscardini L., Rasia E., Tormen G., 2004, MNRAS, 349, 476
Zaroubi S., Branchini E., Hoffman Y., da Costa L. N., 2002, MNRAS, 336, 1234
Zel'dovich Y. B., 1970, A&A, 5, 84

This paper has been typeset from a TEX/LATEX file prepared by the author.